Dynamical density functional theory with hydrodynamic interactions and colloids in unstable traps

M. Rex* and H. Löwen

Institut für Theoretische Physik II: Weiche Materie,
Heinrich-Heine-Universität Düsseldorf, Universitätsstraße 1, D-40225 Düsseldorf, Germany
(Dated: November 2, 2018)

A density functional theory for colloidal dynamics is presented which includes hydrodynamic interactions between the colloidal particles. The theory is applied to the dynamics of colloidal particles in an optical trap which switches periodically in time from a stable to unstable confining potential. In the absence of hydrodynamic interactions, the resulting density breathing mode, exhibits huge oscillations in the trap center which are almost completely damped by hydrodynamic interactions. The predicted dynamical density fields are in good agreement with Brownian dynamics computer simulations.

INTRODUCTION

The dynamics of mesoscopic colloidal particles dispersed in a molecular solvent is of fundamental importance for an understanding of soft matter transport and flow properties. The control over the collective colloidal dynamics leads to the construction of "smart" materials steered by external fields like electro- or magnetorheological fluids [1] and is essential for applications such as gelation and aggregation in paints and cosmetics [2]. Apart from the stochastic Brownian motion of the colloidal particles due to their kicks with the solvent molecules, hydrodynamic interactions between colloidal particles arising from the induced solvent flow field are getting relevant for concentrated suspensions. It has been shown by experiments [3, 4], computer simulations [5, 6] and theory [7, 8, 9, 10] that hydrodynamic interactions can lead to qualitatively different behavior in the bulk transport properties and in colloidal sedimentation as compared to simple Brownian motion valid at very low volume fractions.

A full microscopic theory which starts from the colloidal interactions and their hydrodynamic mobility tensors and predicts the dynamical properties is in principle possible by starting from the Smoluchowski picture [11]. In practice, however, such a predictive theory is hampered by the many-body nature of the problem and the long range of the Oseen mobility tensor which is the leading contribution for a colloidal pair. Explicit approaches have been worked out in the bulk for short-time and long-time diffusion coefficients [7, 8, 9], and for the viscosity [12]. There are also first investigations for colloids near walls and on interfaces [10, 13], and for the nonequilibrium structure of colloids [14] but a general theory for an arbitrary and time-dependent inhomogeneous external potential is missing.

The goal of this letter is twofold: first we construct a dynamical density functional theory [15] which incorporates hydrodynamic interactions. The theory is explicitly worked out for hydrodynamic interactions on the Rotne-Prager level and generalizes earlier formulations [16, 17, 18] where hydrodynamic interactions were neglected. The theory makes predictions for an arbitrary time-dependent external potential, i.e., for a general inhomogeneous nonequilibrium situation. Second, we apply the theory to the dynamics of colloidal particles confined in an unstable optical trap which switches periodically in time from a stable to unstable confining potential. This situation can in principle be realized, e.g., by combining two laser tweezers or by scanning around a single laser tweezer quickly [3, 19, 20]. The response to this oscillating trap is a time-dependent radial-symmetric one-particle density profile which we call - in analogy to trapped Bose gases [21] - a driven *breathing mode*. The periodic breathing mode is interesting in itself since it may serve as a hydrodynamic transmitter [22].

As a result the properties of the breathing mode strongly depend on hydrodynamic interactions. For instance, significant oscillations in the density profile in the trap center which built up if no hydrodynamic interactions are present are completely damped by hydrodynamic interactions. The predictions of the dynamical density functional theory are in very good agreement with Brownian dynamics nonequilibrium computer simulations which take hydrodynamic interactions into account on the same level as the theory does. The theory can in principle be applied to any inhomogeneous situation like laser-induced freezing [23]. It may even be a possible route to incorporate hydrodynamic interactions into dynamical approaches like mode-coupling theory since the latter can be brought into relation with dynamical density functional theory [24].

The starting point of the derivation of the dynamical density functional theory including hydrodynamic interactions on the two-body level is the Smoluchowski equation, i.e., the equation for the time-evolution of the full probability density distribution $P(\mathbf{r}^N, t)$ for N interacting spherical Brownian particles at positions $\mathbf{r}^N =$

$\mathbf{r}_1, \mathbf{r}_2, ..., \mathbf{r}_N$ and time t (see e.g. [11]):

$$\frac{\partial P(\mathbf{r}^N, t)}{\partial t} = \sum_{i,j}^{N} \nabla_i \cdot \mathbf{D}_{ij}(\mathbf{r}^N) \cdot \left[\nabla_j + \frac{\nabla_j U(\mathbf{r}^N, t)}{k_B T} \right] P(\mathbf{r}^N, t),$$
(1)

where $k_B T$ is the thermal energy. We assume pairwise additivity for the total potential energy of the system, such that $U(\mathbf{r}^N, t) = \sum_{k=1}^{N} V_{\text{ext}}(\mathbf{r}_k, t) + \frac{1}{2} \sum_{k=1}^{N} \sum_{l \neq k}^{N} v_2(\mathbf{r}_k, \mathbf{r}_l)$, where $V_{\text{ext}}(\mathbf{r}, t)$ is the one-body time-dependent external potential acting on each particle and $v_2(\mathbf{r}, \mathbf{r}')$ is the pair interaction potential. Hydrodynamic interactions are included through the configuration-dependent diffusion tensor which we approximate on a two particle level: $\mathbf{D}_{ij}(\mathbf{r}^N) \approx D_0 \mathbf{1} \delta_{ij} + D_0 \left[\delta_{ij} \sum_{l \neq i}^{N} \boldsymbol{\omega}_{11}(\mathbf{r}_i - \mathbf{r}_l) + (1 - \delta_{ij}) \boldsymbol{\omega}_{12}(\mathbf{r}_i - \mathbf{r}_j) \right]$. Here, D_0 denotes the diffusion constant of a single isolated particle and δ_{ij} is Kronecker's delta. For a one-component suspension of spheres, series expansions of the two tensors $\boldsymbol{\omega}_{11}$ and $\boldsymbol{\omega}_{12}$ are known, in principle, to arbitrary order [25]. By integrating Eq. (1) with $N \int d\mathbf{r}_2 ... \int d\mathbf{r}_N$, we obtain the equation for the time-evolution of the one-body density $\rho(\mathbf{r}, t)$. The resulting equation depends on both, the time-dependent two-body and the three-body densities. We cast those into a form involving exclusively the equilibrium Helmholtz free energy functional $\mathcal{F}[\rho] = k_B T \int d\mathbf{r} \ \rho(\mathbf{r}, t)[\ln(\Lambda^3 \rho(\mathbf{r}, t)) - 1] + \mathcal{F}_{\text{exc}}[\rho] + \int d\mathbf{r} \ \rho(\mathbf{r}, t) V_{\text{ext}}(\mathbf{r}, t)$, with $\mathcal{F}_{\text{exc}}[\rho]$ being the excess contribution to the free energy functional and Λ the thermal de Broglie wavelength, by making use of static DFT [26] and the first two members of the Yvon-Born-Green (YBG) relations (see, e.g., [27]). To that end, we identify the out-of-equilibrium system at each point in time with an equilibrium reference system whose density profiles are identical. The basic assumption now, which also underlies the original version of the DDFT [16, 17, 18], is to approximate the nonequilibrium two-body and three-body densities by those of the reference system with the same one-body density. Thus, we obtain our central result:

$$\Gamma^{-1} \frac{\partial \rho(\mathbf{r}, t)}{\partial t} = \nabla_\mathbf{r} \cdot \left\{ \rho(\mathbf{r}, t) \nabla_\mathbf{r} \frac{\delta \mathcal{F}[\rho]}{\delta \rho(\mathbf{r}, t)} + \right.$$

$$\int d\mathbf{r}' \ \rho^{(2)}(\mathbf{r}, \mathbf{r}', t) \boldsymbol{\omega}_{11}(\mathbf{r} - \mathbf{r}') \cdot \nabla_\mathbf{r} \frac{\delta \mathcal{F}[\rho]}{\delta \rho(\mathbf{r}, t)} +$$

$$\left. \int d\mathbf{r}' \ \rho^{(2)}(\mathbf{r}, \mathbf{r}', t) \boldsymbol{\omega}_{12}(\mathbf{r} - \mathbf{r}') \cdot \nabla_{\mathbf{r}'} \frac{\delta \mathcal{F}[\rho]}{\delta \rho(\mathbf{r}', t)} \right\}, \quad (2)$$

with the mobility constant Γ for which the Einstein relation gives $D_0/\Gamma = (k_B T)^{-1}$. Eq. (2) has the form of a continuity equation with the current density $\mathbf{j} = \mathbf{j}_1 + \mathbf{j}_2 + \mathbf{j}_3$ given by the terms in the curly brackets. The current density $\mathbf{j}_1$ is proportional to the thermodynamic force $\nabla_\mathbf{r} \frac{\delta \mathcal{F}[\rho]}{\delta \rho(\mathbf{r}, t)}$ and persists when hydrodynamic interactions are neglected [17, 18]. $\mathbf{j}_2$ and $\mathbf{j}_3$ are additional current densities which occur due to the solvent mediated hydrodynamic interactions. $\mathbf{j}_2$ describes the current density stemming from the reflection of the solvent flow induced by the thermodynamic force at position $\mathbf{r}$ on the surrounding particles. $\mathbf{j}_3$, on the other hand, is the current density at position $\mathbf{r}$ due to the solvent flow induced by the thermodynamic force at position $\mathbf{r}'$.

Finally, we close the above relation Eq. (2), which still depends on the nonequilibrium two-body density $\rho^{(2)}(\mathbf{r}, \mathbf{r}', t)$. Within our approximation – the two-body density is assumed to be identical to the equilibrium one of the reference system – it is given at every point in time by the exact generalized Ornstein-Zernike equation [26]:

$$\rho^{(2)}(\mathbf{r}, \mathbf{r}', t) = \rho(\mathbf{r}, t)\rho(\mathbf{r}', t) \left(1 + (k_B T)^{-1} \frac{\delta^2 \mathcal{F}_{\text{exc}}[\rho]}{\delta \rho(\mathbf{r}, t) \delta \rho(\mathbf{r}', t)} \right) +$$

$$\rho(\mathbf{r}', t) \int d\mathbf{r}'' \left\{ (\rho^{(2)}(\mathbf{r}, \mathbf{r}'', t) - \rho(\mathbf{r}, t)\rho(\mathbf{r}'', t)) \right.$$

$$\left. (k_B T)^{-1} \frac{\delta^2 \mathcal{F}_{\text{exc}}[\rho]}{\delta \rho(\mathbf{r}', t) \delta \rho(\mathbf{r}'', t)} \right\}. \quad (3)$$

This implicit equation for the two-body density of the inhomogeneous system may be reasonably approximated by its bulk value [28, 29], i.e.: $\rho^{(2)}(\mathbf{r}, \mathbf{r}', t) \approx \rho(r, t)\rho(r', t)g(|\mathbf{r} - \mathbf{r}'|, \bar{\rho})$, where $g(|\mathbf{r} - \mathbf{r}'|, \bar{\rho})$ is the pair correlation function for a homogeneous system at an appropriately averaged density $\bar{\rho}$. For a hard sphere fluid, an analytic expression for the pair correlation function is available based on the Percus-Yevick equation [30].

We use the method presented here to investigate the time-evolution of the one-body density of a confined cluster of $N = 100$ monodisperse hard spherical particles of diameter σ, which serves as the unit of length henceforth. An appropriate time scale is $\tau_B = \sigma^2/D_0$, and the energy unit is $k_B T$. The particles are trapped in a soft spherical cavity which switches from a stable to an unstable shape periodically in time. The confining external potential only acts on the colloidal particles. Therefore the solvent is treated as an unbounded fluid. The total external potential is modeled as

$$V_{\text{ext}}(r, t) = V_1 \left(\frac{r}{R_1} \right)^4 + V_2 \cos(2\pi t/\tau) \left(\frac{r}{R_2} \right)^2, \quad (4)$$

where $r = |\mathbf{r}|$, $R_1 = 4\sigma$ and $V_1 = 10k_B T$ are the length scale and the strength of an outer fixed cavity and $R_2 = \sigma$ and $V_2 = k_B T$ are the length scale and strength of an inner part, which oscillates in time with a period $\tau = 0.5\tau_B$. A sketch of the setup is shown in Fig. 1. Due to the spherical symmetry, the density profile $\rho(r, t)$ depends only on the radial position coordinate r.

For the hard sphere excess density functional $\mathcal{F}_{\text{exc}}[\rho]$ Rosenfeld's fundamental measure theory [32] was used which provides a very reliable approximation in equilibrium [33]. The distinct hydrodynamic tensor $\boldsymbol{\omega}_{12}(\mathbf{r})$ is approximated by the Rotne-Prager expression [34] $D_0 \boldsymbol{\omega}_{12}(\mathbf{r}) = \frac{3}{8}(\frac{\sigma}{r})[\mathbf{1} + \hat{\mathbf{r}}\hat{\mathbf{r}}] + \frac{1}{16}(\frac{\sigma}{r})^3[\mathbf{1} - 3\hat{\mathbf{r}}\hat{\mathbf{r}}] + \mathcal{O}[(\frac{\sigma}{r})^7]$
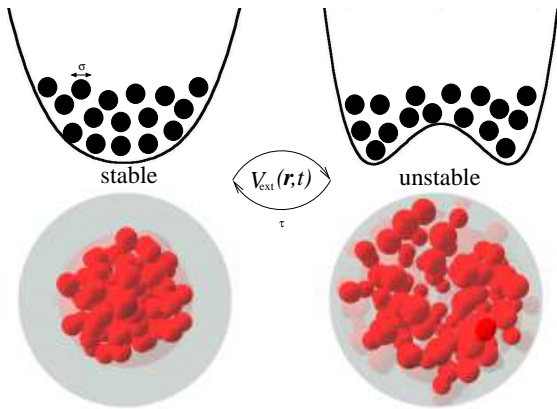
FIG. 1: (Color online) Sketch of the confined system. The external potential models an optical trap $V_{ext}(r,t)$ which changes its central shape from stable to unstable within a time period τ. The trap confines N colloidal hard spheres of diameter σ shown as black circles. Additionally, typical 3d simulation snapshots are shown. The left hand side shows an initial stable configuration for $t = 0$ and the right hand side shows an unstable situation at $t = 2.75\tau_{\mathrm{B}}$ for case (N) [31].

FIG. 2: (Color online) *Steady-state* DDFT (solid curves) and BD (noisy curves) results for the time dependent density profile $\rho(r,t)$. In Fig. (a) and (b) hydrodynamic interactions are taken into account while in (c) and (d) they are neglected. (a) and (c) correspond to the expanding half period and (b) and (d) to the compressing half period, respectively [31]. The profiles correspond to the following time sequence: $t_0 = 2.5\tau_{\mathrm{B}}$, $t_1 = 2.6\tau_{\mathrm{B}}$, $t_2 = 2.7\tau_{\mathrm{B}}$, $t_3 = 2.75\tau_{\mathrm{B}}$ in (a) and (c), and $t_4 = 2.75\tau_{\mathrm{B}}$, $t_5 = 2.85\tau_{\mathrm{B}}$, $t_5 = 2.9\tau_{\mathrm{B}}$, and $t_6 = 3.0\tau_{\mathrm{B}}$.

while the self term $\boldsymbol{\omega}_{11}(\mathbf{r})$ whose leading order term is $\mathcal{O}((\sigma/r)^4)$ is neglected. Here, $\hat{\mathbf{r}} = \mathbf{r}/|\mathbf{r}|$ denotes the unit vector, $\hat{\mathbf{r}}\hat{\mathbf{r}}$ is the dyadic product, and $\mathbf{1}$ is the unit matrix. Thus, on this level of approximation, we incorporate all solvent mediated interactions up to order of $\mathcal{O}((\sigma/r)^3)$. The pair correlation $g(|\mathbf{r} - \mathbf{r}'|, \bar{\rho})$ is calculated at each time step at the average density of the system $\bar{\rho}(t) = 1/R_{\max}(t) \int_0^{R_{\max}(t)} \mathrm{d}r\rho(r,t)$, where $R_{\max}$ is defined by $V_{\mathrm{ext}}(r = R_{\max}(t)) = 10k_{\mathrm{B}}T$.

The results are tested against Brownian dynamics simulations [35] performed on the same level of accuracy of the diffusion tensor, in which the hard interaction is approximated by a slightly softened one:

$$\frac{v_2(r)}{k_{\mathrm{B}}T} = \begin{cases} \left[\left(\frac{\sigma}{r}\right)^{48} - \left(\frac{\sigma}{r}\right)^{24} + \frac{1}{4}\right] & \text{if } r \leq 2^{1/24}\sigma \\ 0 & \text{else} \end{cases} . \quad (5)$$

In all simulations we chose a finite simulation time step of $\Delta t = 10^{-4}\tau_{\mathrm{B}}$. In order to obtain the time-dependent density $\rho(r,t)$ we perform a large number of $N_{\mathrm{run}} = 10^4$ independent runs with different initial configurations sampled from a situation with a static external potential, i.e., Eq. (4) at $t = 0$. Additionally, the densities are compared to those obtained by standard DDFT where hydrodynamic interactions are ignored, i.e., $\boldsymbol{\omega}_{11} = \boldsymbol{\omega}_{12} = 0$. Henceforth, we label the situation including hydrodynamic interactions (H) and the situation where they are neglected (N), respectively. The initial density profile is the equilibrium density profile for $V_{\mathrm{ext}}(r, t = 0)$ calculated from static density functional theory. Typical simulation snapshots are shown in Fig. 1.

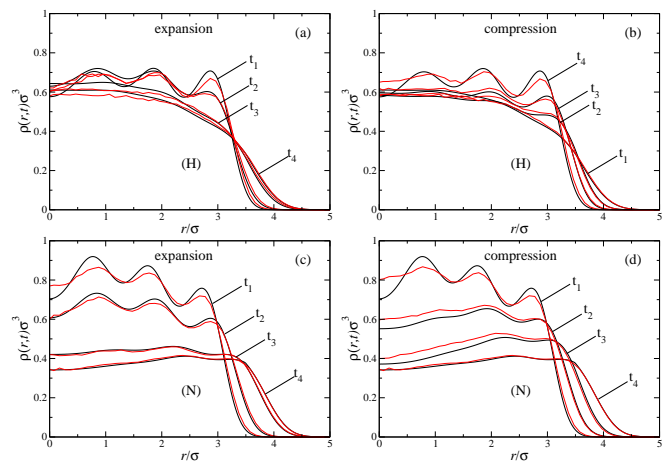The resulting steady-state of the dynamical density profiles, i.e. the driven breathing mode after initial re-laxation, is depicted in Fig. 2. First of all, theory and simulation results are in very good agreement for both situations (H) and (N) but we observe distinct qualitative differences in the breathing mode: Hydrodynamic interactions tend to damp the density response considerably. For neglected hydrodynamic interactions there are huge density oscillations, in particular at the trap center but also at the trap boundaries which are significantly smaller for hydrodynamic interactions. This result is not obvious as hydrodynamic interactions tend to accelerate neighboring particle which are driven into the same direction. The damping effects seen here is caused by the overall motion of the breathing mode which hinders collective streaming due to the counter motion in the opposed part of the trap.

In order to analyze the relaxational behavior towards the steady state, we introduce the second moment of the breathing mode $m_2(t) = \int \mathrm{d}\mathbf{r} \, r^2\rho(r,t)$. It is shown in Fig. 3 in both cases (H) and (N) for DDFT and Brownian Dynamics. Clearly, the dynamic evolution of the second moment is strongly damped by hydrodynamic interactions as revealed by the much slower oscillation amplitude. On top of that the relaxation time towards the steady state breathing mode is considerably larger for hydrodynamic interactions as compared to the simple Brownian case where the relaxation is almost instantaneous. The second moment of the breathing mode is slightly off-phase with respect to the driving external potential $\sim \cos(2\pi t/\tau)$, and the hydrodynamic interactions lead to a stronger phase-shifting.
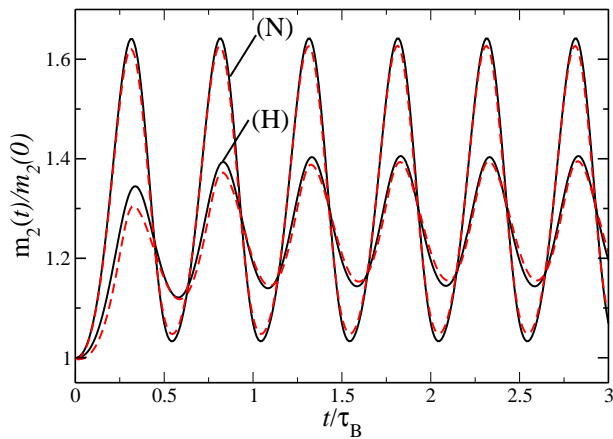
FIG. 3: (Color online) Second moment of the breathing mode, $m_2(t)$, versus time t. DDFT (solid curves) and BD (dashed curves) results for hydrodynamic interactions taken into account (H) and being neglected (N).

In conclusion, we have proposed a dynamical density functional theory which includes hydrodynamic interactions between the colloidal particles and applied it to access the driven breathing mode in oscillating optical traps. The theory was confirmed by Brownian dynamics computer simulations. Hydrodynamic interactions were found to damp the response to the driving trap, to increase the relaxation time towards the steady state and to increase the phase shift. These predictions can in principle be tested by real-space experiments on confined colloidal particles. For charged suspensions, the strength of the hydrodynamic interactions can be systematically tuned in the experiments by varying the colloid charge which governs size of the interactions relative to the physical core which governs the hydrodynamic interactions. It would be interesting to generalize the theory further to orientational degrees of freedom and to self-propelled colloidal particles representing microswimmers where hydrodynamic interactions play a key role.

* Electronic address: rexm@thphy.uni-duesseldorf.de
[1] H. R. Ma, W. J. Wen, W. Y. Tam, and P. Sheng, Adv. in Phys. 52, 343 (2003).
[2] F. Sciortino and P. Tartaglia, Adv. in Phys. 54, 471 (2005).
[3] C. Lutz, M. Reichert, H. Stark, and C. Bechinger, Europhys. Lett. 74, 719 (2006).
[4] A. Banchio, J. Gapinski, A. Patkowski, W. Hauszler, A. Fluerasu, S. Sacanna, P. Holmqvist, G. Meier, M. Lettinga, and G. Nägele, Phys. Rev. Lett. 96, 138303 (2006).
[5] J. T. Padding and A. A. Louis, Phys. Rev. Lett. 93, 220601 (2004).
[6] E. Kuusela, J. M. Lahtinen, and T. Ala-Nissila, Phys. Rev. Lett. 90, 094502 (2003).
[7] G. Nägele and J. K. G. Dhont, J. Chem. Phys. 108, 9566 (1998).
[8] G. Nägele and J. Bergenholtz, J. Chem. Phys. 108, 9893 (1998).
[9] G. Nägele, J. Bergenholtz, and J. K. G. Dhont, J. Chem. Phys. 110, 7037 (1999).
[10] B. Cichocki, M. L. Ekiel-Jezewska, P. Szymczak, and E. Wajnryb, J. Chem. Phys. 117, 1231 (2002).
[11] J. K. G. Dhont, An Introduction to Dynamics of Colloids (Elsevier Science, Amsterdam, 1996).
[12] G. Nägele, J. Phys.: Condens. Matter 15, S407 (2003).
[13] R. Pesché and G. Nägele, Europhys. Lett. 51, 584 (2000).
[14] R. A. Lionberger and W. B. Russel, J. Rheol. 41, 399 (1997).
[15] G. K. L. Chan and R. Finken, Phys. Rev. Lett. 94, 183001 (2005).
[16] A. J. Archer and R. Evans, J. Chem. Phys. 121, 4246 (2004).
[17] U. M. B. Marconi and P. Tarazona, J. Chem. Phys. 110, 8032 (1999).
[18] U. M. B. Marconi and P. Tarazona, J. Phys.: Condens. Matter 12, A413 (2000).
[19] S. Henderson, S. Mitchell, and P. Bartlett, Phys. Rev. Lett. 88, 088302 (2002).
[20] S. Martin, M. Reichert, H. Stark, and T. Gisler, Phys. Rev. Lett. 97, 248301 (2006).
[21] A. Griffin, W. C. Wu, and S. Stringari, Phys. Rev. Lett. 78, 1838 (1997).
[22] G. Guidarelli, F. Craciun, C. Galassi, and E. Roncari, Ultrasonics 36, 467 (1998).
[23] A. Chowdhury, B. J. Ackerson, and N. A. Clark, Phys. Rev. Lett. 55, 833 (1985).
[24] A. J. Archer, J. Phys.: Condens. Matter 18, 5617 (2006).
[25] S. Kim and S. J. Karrila, Microhydrodynamics: Principles and selected applications (Butterworth-Heinemann, Boston, 1991).
[26] R. Evans, Adv. in Phys. 28, 143 (1979).
[27] J. P. Hansen and I. R. MacDonald, Theory of Simple Liquids (Academic, London, 2006), 3rd ed.
[28] S. Dietrich and A. Haase, Phys. Rep. 260, 1 (1995).
[29] B. Götzelmann, A. Haase, and S. Dietrich, Phys. Rev. E 53, 3456 (1996).
[30] A. Trokhymchuk, I. Nezbeda, J. Jirsák, and D. Henderson, J. Chem. Phys. 123, 024501 (2005).
[31] See EPAPS Document No. [] for movies of the time evolution of $\rho(\mathbf{r}, t)$ and typical simulation runs for both setups (H) and (N).
[32] Y. Rosenfeld, Phys. Rev. Lett. 63, 980 (1989).
[33] A. González, J. A. White, F. L. Román, S. Velasco, and R. Evans, Phys. Rev. Lett. 79, 2466 (1997).
[34] J. Rotne and S. Prager, J. Chem. Phys. 50, 4831 (1969).
[35] M. P. Allen and D. J. Tildesley, eds., Computer Simulation of Liquids (Clarendon Press Oxford, Oxford, 1989).